ARTICLES
https://doi.org/10.1038/s41561-019-0320-z
nature geoscience

Methanogenesis sustained by sulfide weathering during the Great Oxidation Event

Shui-Jiong Wang[1*], Roberta L. Rudnick[2,3,4], Richard M. Gaschnig[5], Hao Wang[6] and Laura E. Wasylenki[7,8]

The Great Oxidation Event following the end of the Archaean eon (~2.4 Ga) was a profound turning point in the history of Earth and life, but the relative importance of various contributing factors remains an intriguing puzzle. Controls on methane flux to the atmosphere were of particular consequence; too much methane would have inhibited a persistent rise of O_2, but too little may have plunged Earth into severe and prolonged ice ages. Here, we document a shift in the weathering reactions controlling the ocean-bound flux of nickel—an essential micronutrient for the organisms that produced methane in Precambrian oceans—by applying Ni stable isotope analysis to Mesoarchaean and Palaeoproterozoic glacial sediments. Although Ni flux to the ocean dropped dramatically as Ni content of the continental crust decreased, the onset of sulfide weathering delivered a small, but vital, flux of Ni to the oceans, sustaining sufficient methane production to prevent a permanent icehouse, while allowing O_2 to rise.

For over 50 years, hundreds of researchers have proposed, corroborated, and refuted various possible causes for the Great Oxidation Event (GOE), or the rise in the atmospheric partial pressure of oxygen (P_{O_2}) from <2 ppm to a few percent of the present atmospheric level, roughly 2.4 billion years ago (Ga)[1–4] (Fig. 1a). Several 'whiffs', or transient pulses of oxygenation, are thought to have occurred a bit earlier (2.9–2.5 Ga)[5–7], but conditions were apparently not yet conducive to persistence of free O_2 in the atmosphere. Various late Archaean eon Earth system changes have been proposed as having set the stage for permanent oxygenation, including sufficient H_2 escape from the atmosphere[8], significant growth and compositional change of the continental crust[9–12], and/or a shift from submarine to subaerial volcanism[13,14]. Others argue that the evolution of oxygenic photosynthesis—long thought to have evolved well before the GOE[15–17]—occurred only shortly before 2.3 Ga and directly drove the transformation of Earth's surface[18].

Despite the ongoing debates, consensus holds that one requirement for a lasting rise of O_2 is a dramatic reduction in atmospheric methane—specifically, in the biogenic methane flux to the atmosphere[8,19,20]. Such a drop in methane is consistent with pulses of widespread glaciation recorded between 2.45 and 2.2 Ga[21]; given the faint young Sun, atmospheric methane content was probably a first-order control on surface temperatures. Models by Zahnle et al.[20] of the Archaean–Proterozoic atmospheric transition show the methane mixing ratio dropping around sixfold between 2.6 and 2.4 Ga, before gradually rising again, due to fermentation stimulated by rising O_2-driven primary productivity. Had the methane level dropped less, perhaps the rise of O_2 would not have occurred at this time. Had it dropped more, Earth may have plunged into severe and prolonged ice ages, rather than the few, relatively short-lived events recorded in the rock record. For a planet in mid-life crisis, either extreme would have led to a very different planetary outcome than the one we enjoy. So, what controlled the minimum methane content of the atmosphere during the GOE?

Limitation of methanogenesis followed decrease in Ni supply

Bioavailability of Ni may have been a crucial control on how events unfolded, because Ni is a key metal cofactor in methane-producing enzymes[22]. Having observed a secular trend in Ni/Fe ratios in iron formations through time (Fig. 1b), Konhauser et al.[23,24] estimated that marine Ni concentrations dropped around twofold from 2.7–2.4 Ga and around fivefold by 2.2 Ga. Such a decrease may well have been just enough to induce Ni-limited conditions for methanogens[25]; thus, Konhauser et al.[23,24] surmised that a 'Ni famine' in the Late Archaean oceans severely curbed methanogen productivity, triggering a collapse in atmospheric methane and allowing the GOE to occur. The same general trend in marine Ni concentrations is also recorded in shale- and carbonate-hosted authigenic pyrites[26,27].

Nickel limitation in the Late Archaean oceans is thought to have resulted from weathering of continental crust with decreasing Ni content, when secular cooling of the mantle led to production of less Ni-rich magma over time[23,24,26,27]. Compilations of geochemical data from sedimentary and igneous rocks suggest that the upper continental crust (UCC) also evolved from a mafic bulk composition towards a modern, andesitic composition between 2.7 and 2.5 Ga[9,11,12,28,29], with estimated Ni abundance dropping from >300 to <50 ppm[9,30] (Fig. 1c).

Nickel isotopes imply a change in weathering reactions

Given the scant information available, it is tempting to infer that the flux of Ni to the ocean simply dropped in concert with the Ni content of the exposed crust. However, this cannot be the case, given new evidence from Ni stable isotope analysis of Precambrian glacial

[1]State Key Laboratory of Geological Processes and Mineral Resources, China University of Geosciences, Beijing, China. [2]Department of Earth Science, University of California, Santa Barbara, CA, USA. [3]Earth Research Institute, University of California, Santa Barbara, CA, USA. [4]Department of Geology, University of Maryland, College Park, MD, USA. [5]Department of Environmental, Earth and Atmospheric Sciences, University of Massachusetts Lowell, Lowell, MA, USA. [6]State Key Laboratory of Lithospheric Evolution, Institute of Geology and Geophysics, Chinese Academy of Sciences, Beijing, China. [7]School of Earth and Sustainability, Northern Arizona University, Flagstaff, AZ, USA. [8]Department of Chemistry and Biochemistry, Northern Arizona University, Flagstaff, AZ, USA. *e-mail: wsj@cugb.edu.cn

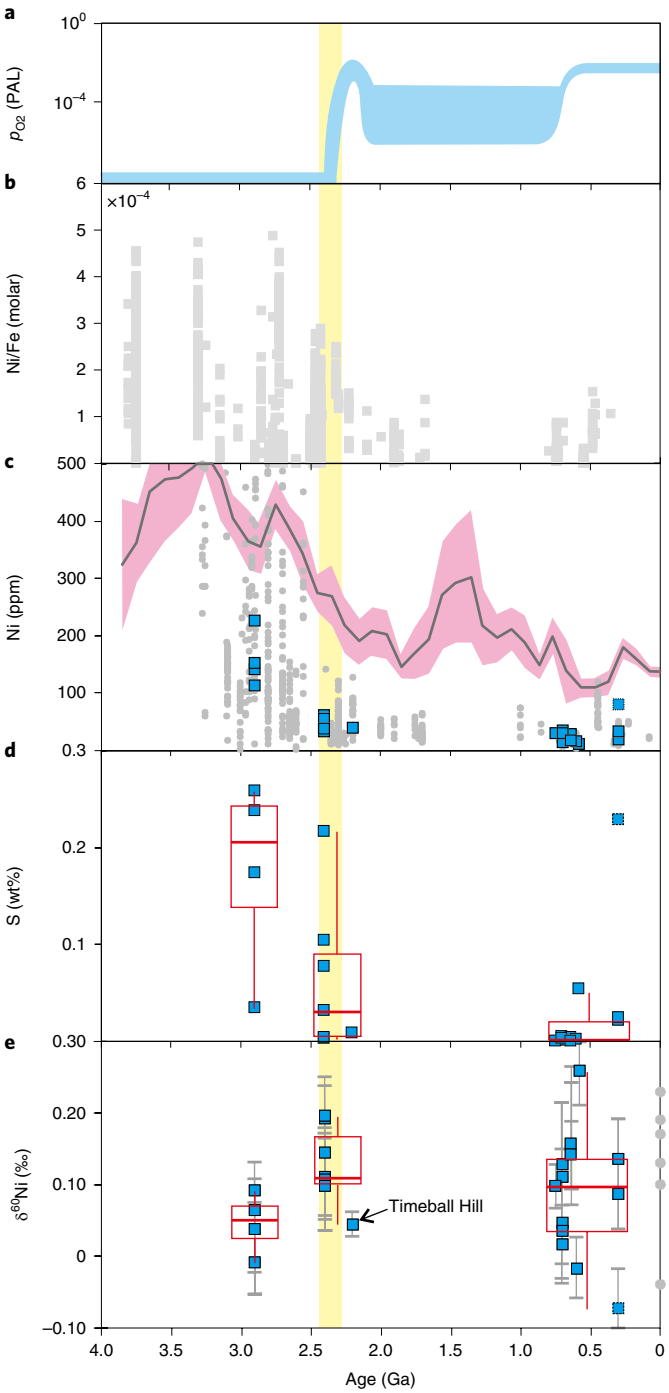

Fig. 1 | Compositional evolution of atmosphere, oceans and continental crust through time. a, A dramatic rise in p_{O_2} (blue curve) from <2 ppm to a few percent of present atmospheric level (PAL) of oxygen occurred ~2.4–2.3 Ga (yellow band)[2]. **b**, By the time p_{O_2} rose, Ni concentrations in seawater, as reflected in Ni/Fe ratios in banded iron formations, were rapidly decreasing[24]. **c**, Temporal trends in Ni concentrations of shales (grey circles)[12], glacial diamictite composites[31] (blue squares) and igneous rocks (black curve with pink uncertainty band, 2 s.e.m.)[9] are consistent with UCC evolution from mafic/ultramafic towards intermediate/felsic bulk compositions between 2.7 and 2.5 Ga. **d**,**e**, Box-and-whisker plots of total sulfur contents and $\delta^{60/58}$Ni values, respectively, of diamictite composites through time. The grey circles in **e** are modern continental sediments[35]. The ends of the boxes are the upper and lower quartiles, while the median is marked by the line inside the box. The ends of the whiskers are the highest and lowest values in each group. Error bars represent 2 s.d.

sediments. Composites of fine-grained matrix from glacial diamictites were prepared previously to serve as proxies for average UCC composition before (~2.9 Ga), across (~2.4–2.2 Ga), and long after (~0.75–0.3 Ga) the GOE (see Supplementary Section 1)[31]. These samples represent mechanically mixed detritus from vast regions of the terrestrial surface, and various weathering indices suggest they probably represent the residues of chemical weathering of the UCC[32]. We find that the Palaeoproterozoic composites (2.4–2.2 Ga) have statistically higher $\delta^{60/58}$Ni values than older samples (Student's *t*-test, $P < 0.05$; $\delta^{60/58}$Ni is the ^{60}Ni/^{58}Ni ratio in parts per thousand, relative to the SRM986 standard; Fig. 1e; also see Supplementary Section 2). The shift is even more significant ($P < 0.01$) if the youngest Palaeoproterozoic composite (Timeball Hill), deposited after the GOE, is not considered (discussed later). What can account for this isotopic shift?

Secular change in the proportions of major igneous lithologies in the UCC, from komatiites to basalts to increasing amounts of trondhjemite–tonalite–granodiorite, cannot explain the new data, as these three crustal components have identical, narrow ranges of $\delta^{60/58}$Ni values within $+0.13 \pm 0.13$‰ (2 s.d.; see Supplementary Fig. 2)[33–35]. A large change in weathering intensity across the GOE is also unlikely to account for the observed isotopic shift, because $\delta^{60/58}$Ni values of Mesoarchaean–Palaeoproterozoic diamictite composites show no correlation with the chemical index of alteration values (an indicator of weathering intensity[36]; Supplementary Fig. 3) and, moreover, leaching of Ni from olivine apparently results in negligible Ni isotope fractionation[37].

Instead, we hypothesize that the shift towards heavier Ni isotope values in the Palaeoproterozoic UCC resulted from the onset of oxidative dissolution of crustal sulfides in the latest Archaean eon. Sulfides are the only major Ni-containing phases that are isotopically distinct from silicates (considerably lighter, at −1.0 to −0.1‰; Supplementary Fig. 2) and were probably stable in the Archaean crust before the rise of oxygen[38]. As the GOE approached, oxidative weathering of the previously untapped inventory of crustal sulfides and acid rock drainage would have released this pool of Ni to rivers and oceans[5,7,39], leaving the weathered UCC and, in turn, the diamictites depleted in light isotopes of Ni. This is corroborated by a drop in the average total sulfur content of the diamictite composites from 2.9 to 2.4–2.2 Ga (Fig. 1d), as well as the disappearance of detrital pyrite from terrestrial sediments across the GOE[38,40], and enrichments of sulfur and chalcophile elements in marine sediments as transient pulses of sulfide weathering began 2.8–2.5 Ga[5,39,41]. Although the total flux of Ni from crust to oceans decreased several-fold from the Mesoarchaean to Palaeoproterozoic, the proportion of Ni flux derived from dissolution of sulfides, rather than silicates, increased significantly, as evidenced by the changing Ni isotopic composition of the weathered UCC.

We note that a new publication[4] reports extraordinarily high sulfur content (1.0–2.5 wt%) in a thin, ~2.45 Ga diamictite layer within the Boolgeeda Iron Formation in Australia. At first glance, such high sulfur in the Palaeoproterozoic diamictites appears to be at odds with our observed trend from higher sulfur in the Mesoarchaean UCC to lower sulfur in the Palaeoproterozoic UCC (Fig. 1d). However, the Boolgeeda diamictite represents a single locality, whereas our diamictite composites, mixed from many samples from four modern continents, more likely reflect the global UCC composition.

Sulfide weathering sustained late Archaean Ni and CH_4 fluxes

With simple mass balance calculations, we can estimate how much the fraction of sulfide-derived Ni entering the oceans may have increased from the Mesoarchaean to the Palaeoproterozoic. These calculations, explained in detail in Supplementary Section 3, account for uncertainties in the range of Ni isotopic compositions

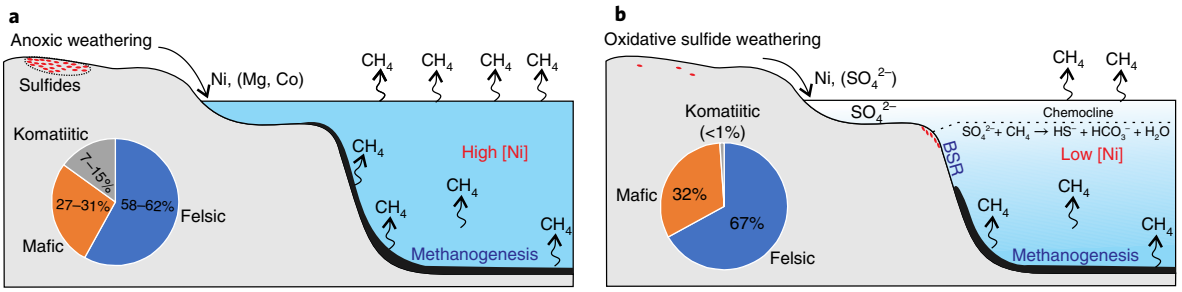

Fig. 2 | Schematic comparison of Ni and methane cycling at different times. a, At 2.9 Ga, silicate weathering of a mafic/ultramafic crust dominated a relatively high Ni flux to the oceans during the Mesoarchaean eon. In the absence of O_2, Ni-bearing sulfide minerals were stable in the crust and retained a significant pool of light Ni isotopes on land. **b**, Between 2.4 and 2.2 Ga, total Ni flux from an increasingly felsic crust dropped dramatically, but oxidative weathering of sulfides sustained a small, but biologically crucial Ni flux to the oceans, probably supporting a low level of methanogenesis. Sulfide weathering, however, also increased sulfate flux, stimulating bacterial sulfate reduction (BSR) and displacing methanogens to deeper waters, while also reducing methane flux to the atmosphere by promoting anaerobic oxidation of methane. The estimated proportions of komatiitic, mafic and felsic components in the crust are from Greber et al.[30].

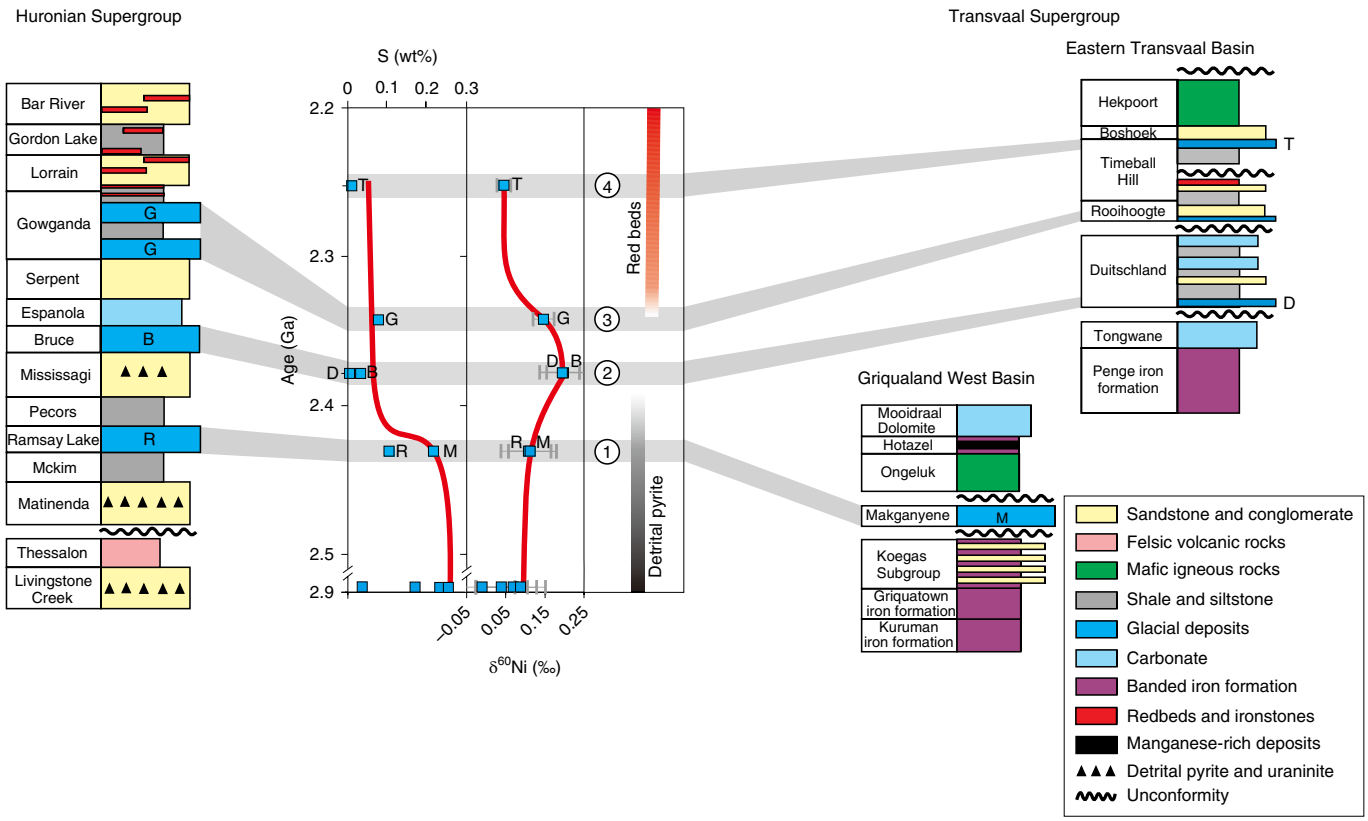

Fig. 3 | Stratigraphic synthesis of the Huronian and Transvaal supergroups, showing trends in total sulfur and $\delta^{60/58}$Ni in composite diamictites. The coupled changes in total sulfur and $\delta^{60/58}$Ni values in the four correlated glacial units with ascending stratigraphic order are consistent with geological redox indicators (that is, the disappearance of detrital pyrite and the appearance of red beds). The timings and correlations of the four glacial events are from Gumsley et al.[44]. First glaciation: Ramsay Lake (R) and Makganyene (M) formations; second glaciation: Bruce (B) and Duitschland (D) formations; third glaciation: Gowganda (G) formation; fourth glaciation: Timeball Hill (T) formation. Error bars represent 2 s.d.

observed in sulfides, the magnitude of the isotopic shift in the diamictites, and the relative fraction of crustal Ni removed by chemical weathering, by varying these parameters systematically. We conclude that the fraction of Ni derived from sulfide weathering probably increased by at least 30% and quite possibly much more, possibly dominating the ocean-bound Ni flux during the GOE (Supplementary Figs. 4 and 5).

Had sulfide weathering not turned on just in time, terrestrial Ni flux to the oceans might have plummeted even more during the GOE. Nickel derived from sulfides may have been the safety net that prevented even more severe Ni limitation of methanogens, which could have plunged Earth into long-lasting icehouse conditions. However, sulfide weathering was a double-edged sword for methanogens. The same reaction that sustained a vital flux of Ni to

the oceans also delivered plenty of sulfate (Fig. 2). Increased sulfate supply would have stimulated bacterial sulfate reduction, which can ecologically outcompete methanogens[42]. Increased sulfate in shallow waters probably also facilitated anaerobic oxidation of methane, thus reducing the rate of methane escape from the water column to the atmosphere[43]. Although the feedback mechanisms are to be discovered, these competing effects of sulfide weathering regulated methane levels during this crucial interval in Earth history, allowing fluxes to drop low enough to promote lasting accumulation of O_2, but keeping them high enough to prevent prolonged or permanent glaciation.

Despite its importance, the outsized role of sulfide weathering in terrestrial Ni flux was probably transient, rather than long lasting. Nickel isotope compositions of globally correlated diamictites deposited during the four Palaeoproterozoic glacial events[44] allow speculation about global shifts in the terrestrial biogeochemical cycle of Ni within the GOE interval (Fig. 3). Early 'whiffs' of atmospheric oxygen[5–7] probably initiated loss of sulfide-hosted Ni from the UCC, resulting in slightly elevated $\delta^{60/58}$Ni values (+0.11‰) relative to the Mesoarchaean samples in crustal residues sampled by the first glacial event (~2.43 Ga). Sulfide phases were only beginning to dissolve from the crust at this stage, as evidenced by the relatively high total sulfur contents of these glacial sediments and the persistence of detrital pyrite grains in the overlying stratigraphic unit[4,45]. Over time, as the reservoir of crustal sulfides continued to react with oxygen, total sulfur contents dropped and $\delta^{60/58}$Ni continued to rise (+0.20‰), as illustrated by weathering residues from the second glacial event. Eventually, sulfide weathering may have reached a quasi-steady state, when the backlog of easily oxidizable sulfides in the UCC diminished. Detrital pyrite disappeared from the UCC by the third glacial event, and the $\delta^{60/58}$Ni decreased a bit (+0.14‰), implying a lower fraction of Ni flux derived from sulfides.

Red beds retained isotopically light Ni on lands after the GOE

Another phenomenon developed on land on the newly oxidized planetary surface, changing once more the controls on the distribution of Ni and its isotope ratios. Continental red beds—sedimentary rocks stained red by iron oxyhydroxides—began to form at the end of the third glacial event during the GOE (Fig. 3)[18]. Recent field and experimental studies show that iron oxyhydroxides preferentially incorporate light Ni isotopes relative to ambient fluids[37,46,47]. In today's fully oxic world, retention of isotopically light Ni in iron-rich soils leads to an isotopically heavy dissolved Ni flux to rivers and oceans[37,48,49]. This process probably began to affect the terrestrial Ni cycle to some extent in the Palaeoproterozoic and could account for the lower Ni isotope value (+0.04‰) in the weathered residue from the fourth glacial event, when red beds were well developed[18,50]. This mechanism can also explain the variably low Ni isotope values and weak, negative correlation between $\delta^{60/58}$Ni and Th/U values observed in much younger, Neoproterozoic–Palaeozoic diamictite composites (Supplementary Fig. 6); continental areas that experienced greater extents of oxidative weathering (for example, high Th/U) are more depleted in heavy Ni isotopes.

Our findings provide a new perspective on the role of sulfide weathering in ecosystem–climate systems during the GOE. The evidence presented here indicates that the bioavailable Ni supply of the ocean during this crucial interval derived largely from sulfide weathering. Ironically, conventional wisdom is that sulfide weathering inhibits methanogenesis[20], but, in this case, it probably helped sustain methanogen productivity and indirectly prevented a prolonged icehouse. Analysis of additional proxies and modelling efforts could test this hypothesis and also evaluate whether varying rates of sulfide weathering between 2.4 and 2.2 Ga were genetically related to atmospheric oxygen oscillations as well as the onset and termination of multiple glacial events. Better constraints on sulfide weathering rates could also lead to more robust estimates of Palaeoproterozoic p_{O_2}.

Online content

Any methods, additional references, Nature Research reporting summaries, source data, statements of data availability and associated accession codes are available at https://doi.org/10.1038/s41561-019-0320-z.

Received: 18 May 2018; Accepted: 2 February 2019;
Published online: 4 March 2019

References

1. Holland, H. D. The oxygenation of the atmosphere and oceans. *Phil. Trans. R. Soc. Lond. B* **361**, 903–915 (2006).
2. Lyons, T. W., Reinhard, C. T. & Planavsky, N. J. The rise of oxygen in Earth's early ocean and atmosphere. *Nature* **506**, 307–315 (2014).
3. Farquhar, J., Bao, H. & Thiemens, M. J. S. Atmospheric influence of Earth's earliest sulfur cycle. *Science* **289**, 756–758 (2000).
4. Philippot, P. et al. Globally asynchronous sulphur isotope signals require re-definition of the Great Oxidation Event. *Nat. Commun.* **9**, 2245 (2018).
5. Anbar, A. D. et al. A whiff of oxygen before the Great Oxidation Event? *Science* **317**, 1903–1906 (2007).
6. Crowe, S. A. et al. Atmospheric oxygenation three billion years ago. *Nature* **501**, 535–538 (2013).
7. Reinhard, C. T., Raiswell, R., Scott, C., Anbar, A. D. & Lyons, T. W. A late Archean sulfidic sea stimulated by early oxidative weathering of the continents. *Science* **326**, 713–716 (2009).
8. Catling, D. C., Zahnle, K. J. & McKay, C. P. Biogenic methane, hydrogen escape, and the irreversible oxidation of early Earth. *Science* **293**, 839–843 (2001).
9. Keller, C. B. & Schoene, B. Statistical geochemistry reveals disruption in secular lithospheric evolution about 2.5 Gyr ago. *Nature* **485**, 490–493 (2012).
10. Lee, C.-T. A. et al. Two-step rise of atmospheric oxygen linked to the growth of continents. *Nat. Geosci.* **9**, 417–424 (2016).
11. Smit, M. A. & Mezger, K. Earth's early O_2 cycle suppressed by primitive continents. *Nat. Geosci.* **10**, 788–792 (2017).
12. Tang, M., Chen, K. & Rudnick, R. L. Archean upper crust transition from mafic to felsic marks the onset of plate tectonics. *Science* **351**, 372–375 (2016).
13. Kump, L. R. & Barley, M. E. Increased subaerial volcanism and the rise of atmospheric oxygen 2.5 billion years ago. *Nature* **448**, 1033–1036 (2007).
14. Gaillard, F., Scaillet, B. & Arndt, N. T. Atmospheric oxygenation caused by a change in volcanic degassing pressure. *Nature* **478**, 229–232 (2011).
15. Buick, R. When did oxygenic photosynthesis evolve? *Phil. Trans. R. Soc. Lond. B* **363**, 2731–2743 (2008).
16. Planavsky, N. J. et al. Evidence for oxygenic photosynthesis half a billion years before the Great Oxidation Event. *Nat. Geosci.* **7**, 283–286 (2014).
17. Lalonde, S. V. & Konhauser, K. O. Benthic perspective on Earth's oldest evidence for oxygenic photosynthesis. *Proc. Natl Acad. Sci. USA* **112**, 995–1000 (2015).
18. Kopp, R. E., Kirschvink, J. L., Hilburn, I. A. & Nash, C. Z. The Paleoproterozoic snowball Earth: a climate disaster triggered by the evolution of oxygenic photosynthesis. *Proc. Natl Acad. Sci. USA* **102**, 11131–11136 (2005).
19. Kasting, J. F. Methane and climate during the Precambrian era. *Precambrian Res.* **137**, 119–129 (2005).
20. Zahnle, K., Claire, M. & Catling, D. The loss of mass-independent fractionation in sulfur due to a Palaeoproterozoic collapse of atmospheric methane. *Geobiology* **4**, 271–283 (2006).
21. Evans, D., Beukes, N. & Kirschvink, J. Low-latitude glaciation in the Palaeoproterozoic era. *Nature* **386**, 262–266 (1997).
22. Thauer, R. K. Biochemistry of methanogenesis: a tribute to Marjory Stephenson: 1998 Marjory Stephenson prize lecture. *Microbiology* **144**, 2377–2406 (1998).
23. Konhauser, K. O. et al. Oceanic nickel depletion and a methanogen famine before the Great Oxidation Event. *Nature* **458**, 750–753 (2009).
24. Konhauser, K. O. et al. The Archean nickel famine revisited. *Astrobiology* **15**, 804–815 (2015).
25. Glass, J. & Dupont, C. *The Biological Chemistry of Nickel* 12–26 (Royal Society of Chemistry, 2017).
26. Large, R. R. et al. Trace element content of sedimentary pyrite as a new proxy for deep-time ocean–atmosphere evolution. *Earth Planet. Sci. Lett.* **389**, 209–220 (2014).
27. Gallagher, M., Turner, E. & Kamber, B. In situ trace metal analysis of Neoarchaean—Ordovician shallow-marine microbial-carbonate-hosted pyrites. *Geobiology* **13**, 316–339 (2015).

28. Condie, K. C. Chemical composition and evolution of the upper continental crust: contrasting results from surface samples and shales. *Chem. Geol.* **104**, 1–37 (1993).
29. Taylor, S. & McLennan, S. *The Continental Crust: Its Evolution Composition* (Blackwell, London, 1985).
30. Greber, N. D. et al. Titanium isotopic evidence for felsic crust and plate tectonics 3.5 billion years ago. *Science* **357**, 1271–1274 (2017).
31. Gaschnig, R. M. et al. Compositional evolution of the upper continental crust through time, as constrained by ancient glacial diamictites. *Geochim. Cosmochim. Acta* **186**, 316–343 (2016).
32. Li, S., Gaschnig, R. M. & Rudnick, R. L. Insights into chemical weathering of the upper continental crust from the geochemistry of ancient glacial diamictites. *Geochim. Cosmochim. Acta* **176**, 96–117 (2016).
33. Gueguen, B., Rouxel, O., Ponzevera, E., Bekker, A. & Fouquet, Y. Nickel isotope variations in terrestrial silicate rocks and geological reference materials measured by MC-ICP-MS. *Geostand. Geoanal. Res.* **37**, 297–317 (2013).
34. Hofmann, A. et al. Comparing orthomagmatic and hydrothermal mineralization models for komatiite-hosted nickel deposits in Zimbabwe using multiple-sulfur, iron, and nickel isotope data. *Miner. Deposita* **49**, 75–100 (2014).
35. Cameron, V., Vance, D., Archer, C. & House, C. H. A biomarker based on the stable isotopes of nickel. *Proc. Natl Acad. Sci. USA* **106**, 10944–10948 (2009).
36. Nesbitt, H. & Young, G. Early Proterozoic climates and plate motions inferred from major element chemistry of lutites. *Nature* **299**, 715–717 (1982).
37. Spivak-Birndorf, L. J., Wang, S.-J., Bish, D. L. & Wasylenki, L. E. Nickel isotope fractionation during continental weathering. *Chem. Geol.* **476**, 316–326 (2017).
38. Johnson, J. E., Gerpheide, A., Lamb, M. P. & Fischer, W. W. O_2 constraints from Paleoproterozoic detrital pyrite and uraninite. *Geol. Soc. Am. Bull.* **126**, 813–830 (2014).
39. Konhauser, K. O. et al. Aerobic bacterial pyrite oxidation and acid rock drainage during the Great Oxidation Event. *Nature* **478**, 369–373 (2011).
40. Holland, H. D. *The Chemical Evolution of the Atmosphere and Oceans* (Princeton Univ. Press, 1984).
41. Stüeken, E. E., Catling, D. C. & Buick, R. Contributions to late Archaean sulphur cycling by life on land. *Nat. Geosci.* **5**, 722–725 (2012).
42. Lovley, D. R. & Klug, M. J. Sulfate reducers can outcompete methanogens at freshwater sulfate concentrations. *Appl. Env. Microbiol.* **45**, 187–192 (1983).
43. Catling, D., Claire, M. & Zahnle, K. Anaerobic methanotrophy and the rise of atmospheric oxygen. *Phil. Trans. A Math. Phys. Eng. Sci.* **365**, 1867–1888 (2007).
44. Gumsley, A. P. et al. Timing and tempo of the Great Oxidation Event. *Proc. Natl Acad. Sci. USA* **114**, 1811–1816 (2017).
45. Ulrich, T., Long, D., Kamber, B. & Whitehouse, M. In situ trace element and sulfur isotope analysis of pyrite in a Paleoproterozoic gold placer deposit, Pardo and Clement Townships, Ontario, Canada. *Econ. Geol.* **106**, 667–686 (2011).
46. Wang, S.-J. & Wasylenki, L. E. Experimental constraints on reconstruction of Archean seawater Ni isotopic composition from banded iron formations. *Geochim. Cosmochim. Acta* **206**, 137–150 (2017).
47. Wasylenki, L. E., Howe, H. D., Spivak-Birndorf, L. J. & Bish, D. L. Ni isotope fractionation during sorption to ferrihydrite: implications for Ni in banded iron formations. *Chem. Geol.* **400**, 56–64 (2015).
48. Cameron, V. & Vance, D. Heavy nickel isotope compositions in rivers and the oceans. *Geochim. Cosmochim. Acta* **128**, 195–211 (2014).
49. Ratié, G. et al. Nickel isotope fractionation during tropical weathering of ultramafic rocks. *Chem. Geol.* **402**, 68–76 (2015).
50. Coetzee, L., Beukes, N., Gutzmer, J. & Kakegawa, T. Links of organic carbon cycling and burial to depositional depth gradients and establishment of a snowball Earth at 2.3 Ga. Evidence from the Timeball Hill Formation, Transvaal Supergroup, South Africa. *S. Afr. J. Geol.* **109**, 109–122 (2006).

Acknowledgements

We thank W. Maier and E. Ripley for providing the komatiite samples. The research was supported by the National Science Foundation EAR-1424676 to L.E.W. and EAR-1321954 to R.L.R. and R.M.G.

Author contributions

S.-J.W. conceived the project, conducted the experimental analyses, interpreted the data and drafted the manuscript. L.E.W. provided funding and facilities, augmented the data interpretation and substantially edited the manuscript. R.L.R., R.M.G. and H.W. provided samples and participated in discussion of the interpretations and manuscript editing.

Competing interests

The authors declare no competing interests.

Additional information

Supplementary information is available for this paper at https://doi.org/10.1038/s41561-019-0320-z.

Reprints and permissions information is available at www.nature.com/reprints.

Correspondence and requests for materials should be addressed to S.-J.W.

Methods

Nickel isotope analyses. Approximately 100–300 mg of composite powders were digested in a mixture of distilled HF + HNO_3 + HCl. After complete dissolution, aliquots of sample solutions containing ~1.5 μg Ni were spiked with a ^{61}Ni–^{62}Ni double spike to reach an optimum spike-to-sample ratio of 64:36. The spiked solutions were refluxed to ensure sample–spike equilibration before column chemistry.

Separation of Ni from the matrices was achieved using a three-stage, cation exchange chromatography procedure using Bio-Rad 200–400 mesh AG 50W-X8 resin. The first column separated iron, manganese, and chromium from nickel using a mixture of 20% 10 M HCl and 80% acetone. The second column used 15% 10 M HCl and 85% acetic acid to separate Ni from elements such as magnesium, calcium, aluminium and titanium. The third column further purified Ni using 0.9 M HNO_3 to remove sodium and potassium. Five United States Geological Survey (USGS) standards (Nod-A-1, BIR-1, BHVO-1, SCO-1 and SDO-1) were processed, together with samples, for column chemistry. The yield was >85% and the total procedural blank was <10 ng, which was negligible compared with the >2.5 μg of Ni in the samples

Nickel isotopic ratios were measured using a Nu Plasma II multicollector inductively coupled plasma mass spectrometer at Indiana University with an Aridus II desolvating nebulizer. Four Ni isotopes (^{58}Ni, ^{60}Ni, ^{61}Ni and ^{62}Ni) were measured simultaneously on Faraday cups. ^{57}Fe was also measured and used to correct for interference on ^{58}Ni, although this correction was always very small. The background for ^{60}Ni was $<10^{-3}$ V, which is negligible relative to sample signals of ~3–4 V. Each sample solution and the five USGS standards were measured four times on different days, and the raw data were processed using the double-spike equations to correct for isotope fractionation caused by instrument-induced mass bias and imperfect column yields. The Ni isotopic results were reported in the conventional δ notation in per mille relative to National Institute of Standards and Technology standard reference material (SRM) 986: $\delta^{60/58}Ni = [(^{60}Ni/^{58}Ni_{sample})/(^{60}Ni/^{58}Ni_{SRM986}) - 1] \times 1{,}000$. The five USGS standards yielded $\delta^{60/58}$Ni values of +1.10 ± 0.07‰ for Nod-A-1, +0.12 ± 0.03‰ for BIR-1, +0.03 ± 0.03‰ for BHVO-1, +0.08 ± 0.07‰ for SCO-1 and +0.60 ± 0.05‰ for SDO-1 (Supplementary Table 2).

Total sulfur analyses. Total sulfur was determined using a LECO SC832 in the Indiana Geological and Water Survey at Indiana University. Approximately 100–300 mg powder for each sample was weighed into a ceramic boat with an open surface area, and the total sulfur content was measured by infrared absorption, following combustion of the sample powder in an oxygen-rich environment. The standard, LECO 502-320, yielded a value of 2.23 ± 0.06%.

Data availability

All data supporting the findings of this study are available within the main text, figures and Supplementary Information files.